Improving Distributed Fiber-Optic Sensor Measures by Digital Image Correlation: Two-Stage Structural Health Monitoring

ACI STRUCTURAL JOURNAL TECHNICAL PAPER

Title No. 118-S117

Improving Distributed Fiber-Optic Sensor Measures by Digital Image Correlation: Two-Stage Structural Health Monitoring

by Maurizio Morgese, Marco Domaneschi, Farhad Ansari, Gian Paolo Cimellaro, and Daniele Inaudi

This paper deals with the integrated use of distributed fiber-optic sensors and digital image correlation techniques to develop a two-stage monitoring method for damage detection, localization, and quantification. The proposed methodology was applied in the laboratory on reinforced concrete beam specimens and is suitable for further field developments in concrete structures of large dimensions. The first stage is based on distributed strain monitoring through Brillouin scattering-based fiber-optic sensors to detect and locate potential damage zones within the entire structure, while the second focuses on verification of the critical regions identified by the optical-fiber sensor using the digital image correlation technique.

Keywords: cracks; digital image correlation (DIC); fiber-optic sensors (FOSs); reinforced concrete (RC) elements; structural health monitoring (SHM).

INTRODUCTION

Many countries around the world are facing serious problems with the aging of infrastructures. Besides the degradation process that is usually associated with aging, it is also important to consider the design standards that were originally used. Indeed, more updated regulations may have come into force, including methodologies unknown or impossible to apply at the time when the infrastructure was designed.

In this context, most of the bridges built after 1945 were designed with a service life of 50 to 100 years, many of which are still operational today, but with many uncertainties about their safety performance. In 2001, the European Union-funded BRIME project identified that highway bridges in three different European countries (France, Germany, and the United Kingdom) present deficiencies at a rate of 39%, 30%, and 37%, respectively, with the main cause being the corrosion of reinforcement.[1] In Germany, for example, the federal government through the Federal Highway Research Institute is monitoring 39,621 bridges, of which 10.6% are in a condition that is not satisfactory and 1.8% are in poor condition, needing an urgent repair, according to the statistics reported by *The New York Times*.[2] Similarly, according to the 2013 ASCE Report Card, in the United States, a significant portion of infrastructures have exceeded their design service life, showing evidence of aging and deterioration.[3]

Despite the modern practices in the design of bridges, the increased frequency of extreme events such as earthquakes and hurricanes renders them unsafe unless their conditions are properly monitored.[4] Therefore, structural health monitoring (SHM) has been identified as one of the possible alternatives or complements to visual inspections because of its higher reliability and accuracy for assessing conditions due to access to quantitative information.[5] In essence, real-time monitoring of structures will prevent the imminence of collapse by the early detection of anomalies.[6] The information obtained from SHM provides valuable information for undertaking remedial actions and assuring the safety of structures. Furthermore, sensor-based quantitative monitoring of structures will be essential in reducing the life cycle costs in the maintenance of structures and adds to the knowledge base pertaining to structural behavior.[7] In the United States, several SHM programs have been established for the installation of monitoring systems on major high-rise buildings, bridges, and dams, with special attention to the seismic and coastal regions. Table 1 provides a list of the major monitored bridges, which have been instrumented by using traditional sensors such as displacement transducers, strain gauges, and accelerometers.[3]

Damage conditions in bridge structures may lead to failure of structural components up to collapse; therefore, several SHM techniques have been implemented to prevent such failures. Nondestructive and non-contact methods are of special concern with respect to other solutions because they do not affect the structural performance.[8] A nondestructive method to detect cracks may be based on distributed strain monitoring along the main span by using Brillouin scattering-based optical-fiber sensors.[9] Indeed, this new generation of optical fibers makes possible innovative sensing solutions for SHM.[10,11]

Monitoring large-size civil structures represents a challenging task. Discrete sensors such as strain gauges can detect damage near the areas where they are located. Distributed optical sensors provide a high-density sensing network to cover the entire structure, collecting strain data all along the optical fiber.[12] A review of technical literature reveals that fiber-optic sensors (FOSs) have been predominantly employed in bridges. Among the notable bridges monitored by FOS, the Brooklyn Bridge in New York City provides a

ACI Structural Journal, V. 118, No. 6, November 2021.

MS No. S-2020-198.R2, doi: 10.14359/51732994, received November 19, 2020, and reviewed under Institute publication policies.

Table 1—Major instrumented bridges in United States

Name	Year	Location	Type
Golden Gate Bridge	1937	San Francisco, CA	Suspension
Vincent Thomas Bridge	1964	Los Angeles, CA	Suspension
Commodore Barry Bridge	1974	Pennsylvania/New Jersey	Truss
Sunshine Skyway Bridge	1987	Terra Ceia, FL	Cable-stayed
Fred Hartman Bridge	1995	La Porte, TX	Cable-stayed
Bill Emerson Memorial Bridge	2003	Missouri/Illinois	Cable-stayed
Alfred Zampa Memorial Bridge	2003	Vallejo, CA	Suspension
I-35W Saint Anthony Falls Bridge	2008	Minneapolis, MN	Post-tensioned concrete box girder

good example, where the cracking of the crests in its double-span masonry vaults were investigated by serially multiplexed fiber Bragg grating (FBG) crack, temperature, and tilt sensors.[13] The yearlong, daily, real-time monitoring of the bridge revealed seasonal thermal fluctuations as the cause for the vault cracks. The masonry vaults were immediately rehabilitated following these findings. The Taylor Bridge in Manitoba, Canada, is another example, where the bridge was fully instrumented with 63 FBG and distributed sensors along its span.[14] Sixty percent of the properly sealed strain gauges malfunctioned due to excessive moisture resulting from the steam-curing process, while distributed FOSs were not affected and all survived. This confirms the distributed FOSs' compatibility with concrete and their potential as preferred sensors in SHM.[14]

Another example of a bridge monitored by FOSs is the Kishwaukee River Bridge (Illinois). Analysis of the results led to the identification of five locations with anomalies. Visual inspection verified the presence of two microcracks and three misaligned sections at the shear keys of the box segments.[9] Results of another study further verified the capability of distributed optical-fiber sensors in reference-free dynamic health monitoring of bridges subjected to truck traffic.[15] Reference-free monitoring of damage under operating traffic conditions provides opportunities for the practical application of distributed sensors for condition assessment of bridges without prior knowledge of their condition.

In Europe, SHM with FOSs has been studied in projects as Sustainable Bridges[16] and COST.[17]

Among the nondestructive methods, digital image correlation (DIC) could be an easier, low-priced, and competitive monitoring technique. Furthermore, it belongs to the class of non-contact and material-independent monitoring techniques. Indeed, it provides a full-field displacements and deformations measurement through image processing that would be equivalent to the installation of several sensors in a two-dimensional domain.[18] These features are fundamental for the detection of damage in quasi-brittle materials like concrete, where fracture usually develops as local microcracks that may come together to form a macrocrack, seriously affecting the performance of the whole structure.[19] It has been demonstrated that DIC can locate invisible cracks in concrete, quantify their openings, and also measure point displacements and local deformations.[20] DIC does need a stable, non-vibrating support, but if this condition is fulfilled, it can be successfully used also in fatigue[21] and for full-scale tests to failure of bridges.[22]

The present contribution explores the feasibility of hybrid approaches for damage detection to localization and quantification in concrete structures. These aspects are examined by laboratory tests. In particular, it deepens the advantages of the integrated use of distributed FOS and DIC techniques to develop a two-stage monitoring and inspection method potentially suitable for large-scale concrete structures. The first stage is based on strain monitoring through distributed FOSs to detect and locate unusual behaviors on the reinforced concrete (RC) beams. The second stage is implemented for damage quantification by using DIC.

Focusing on installation costs, the one-time original cost of the distributed FOS sensing system is higher compared with the cost of conventional local sensor equipment installation.[23] However, in terms of costs associated with installation duration, computational efforts, sensors, and materials, distributed sensing has a lower cost. The second-stage monitoring system is non-contact, so it does not need special installation techniques. Therefore, by combining the two monitoring methods, as specified in this work, it may be possible to achieve a great compromise between total installation costs and the accuracy of results.

An experimental study through four-point bending tests on two RC beam specimens was performed to find out valuable information about potential damage detection and localization by FOS distributed sensing, while the DIC technique has been implemented locally to quantify cracks. The basic theoretical knowledge of the selected techniques is introduced in the next sections, along with the methodology. The beam specimens and the design of the test are then presented with the analysis of the results and their discussion.

RESEARCH SIGNIFICANCE

This work provides an advancement from damage detection to localization and quantification that could be exploited from laboratory applications to field applications for long-span concrete structures.[24] It deepens the advantages of the integrated use of distributed FOS and DIC techniques to develop a two-stage monitoring and inspection approach. Their combined use may be possible to achieve a great compromise between total cost installation and accuracy of results. The two-stage SHM method proves effective in laboratory RC specimens in detecting, locating, and quantifying the presence of cracks of the same size as those that can be

measured in real conditions on concrete structures of large dimensions.

Digital image correlation technique

Digital image correlation (DIC) is an effective and widely used non-contact and material-independent technique for measuring material deformation.[25] It was originally developed by Sutton et al.[26] in the 1980s, and it is widely used for full-field deformation measurements due to its advantages of simple equipment and high precision. The principle of DIC is based on two key technologies: a camera to take images at different conditions, and a DIC algorithm.

Considerable progress has been made in recent decades in both developing new experimental DIC techniques and in enhancing the performance of the relevant computational algorithms.[27-34] Nowadays, there are some commercial two-dimensional (2-D) and three-dimensional (3-D) DIC systems on the market, but these systems are usually too expensive for many research institutes to afford. The development of a low-cost DIC system such as NCORR or XJTUDIC is of special interest.[35] In particular, the high-quality, flexible DIC software package called NCORR can be used to trace the displacement field (u, v) and the related deformations in small and finite deformations, accounting for discontinuities as well (cracking).[36]

Two-dimensional DIC using a single fixed camera is employed to measure plan deformations on external surfaces. The details of the monitoring system can be found in Sutton et al.[37] Three-dimensional DIC is developed to get the 3-D deformation field and is based on the principle of binocular stereovision.[38-41] The 2-D DIC, using a single fixed camera, is adopted for the laboratory experimental tests on RC beam specimens. The measurements are limited to the plane deformation field on the lateral surface of the specimens. It consists of the following three steps:

1. Specimen and experimental preparations with the application of a speckle pattern;
2. Recording images at different loading steps from the initial reference condition; and
3. Processing of the collected images to obtain the displacement and deformation fields.

Figure 1 shows the experimental setup for the 2-D DIC. Random gray intensity distribution (that is, random speckle pattern) has to be applied on the specimen surface. The pattern deforms together with the specimen and allows the DIC algorithm to the reference to compute both the displacement and the deformation fields. The specimen surface has to be prepared flat and to remain on the same plane parallel to the charge-coupled device (CCD) of the camera. Furthermore, the system should not suffer from geometric distortion; otherwise, correction techniques should be applied.[42-48] Alternatively, laser speckle-based techniques have been developed to avoid the physical establishment of speckle patterns on the surface of concrete.[49-51]

Image processing algorithms are used to track the relative displacements of material points between a reference image and the current one. In recent years, computation algorithms have improved, and the NCORR open-source one was used in this study. It is implemented in MATLAB and

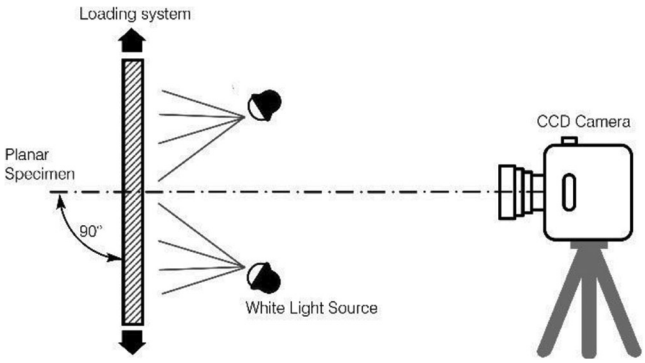

Fig. 1—Experimental setup for 2-D DIC.

can be adapted to the user's needs.[36] The reference image is partitioned into subsets. A homogeneous deformation field is assumed for each subset. Within the NCORR process, the subdomains are initially a contiguous circular group of points that are on integer pixel locations in the reference configuration. A linear first-order transformation is used to transform the coordinates of these points from the reference to the current configuration

$$\begin{cases} \tilde{x}_{cur_i} = x_{ref_i} + u_{rc} + \dfrac{\partial u}{\partial x_{rc}}\left(x_{ref_i} - x_{ref_c}\right) + \dfrac{\partial u}{\partial y_{rc}}\left(y_{ref_j} - y_{ref_c}\right) \\ \tilde{y}_{cur_i} = y_{ref_i} + v_{rc} + \dfrac{\partial v}{\partial x_{rc}}\left(x_{ref_i} - x_{ref_c}\right) + \dfrac{\partial v}{\partial y_{rc}}\left(y_{ref_j} - y_{ref_c}\right) \end{cases} (i,j) \in S \tag{1}$$

$$p = \left\{ u \quad v \quad \frac{\partial u}{\partial x} \quad \frac{\partial u}{\partial y} \quad \frac{\partial v}{\partial x} \quad \frac{\partial v}{\partial y} \right\}^T \tag{2}$$

In Eq. (1), x_{ref_i} and y_{ref_j} are the x- and y-coordinates of an initial reference subset point, while the coordinates of the center of the initial reference subset are x_{ref_c} and y_{ref_c}, whereas $\tilde{x}_{cur_i}$ and $\tilde{y}_{cur_i}$ are the coordinates of a current subset point. The generalized deformation vector is defined by Eq. (2). The relative location of the points with respect to the center of the subset is indicated by indexes (i, j); S comprehends all of the subset points. The transformation from the reference to the current coordinate system is highlighted by the subscript rc. The strain field is noise sensitive because strain computation implies displacement differentiation. In Pan et al.,[52] the NCORR algorithm is introduced to compute the displacement gradients to compensate noise. More details on the algorithm can be found in Blaber et al.[36]

Distributed fiber-optic sensors

Civil infrastructures are usually characterized by their oversized dimensions that do not allow for conventional point-mode monitoring techniques; therefore, the use of distributed optical fiber optic systems has increased over time for the detection of anomalies and cracks in civil engineering. As shown in Fig. 2, a single FOS cable sensor can be applied throughout the entire structure length, surface, or volume, creating a powerful approach for global and yet detailed condition assessment of structures. In addition, other attributes of optical fibers which contribute to the effective

detection of damage in concrete structures are geometric adaptability, immunity to electrical and magnetic interference, high resolution, and a high signal-to-noise ratio.[53]

Shi et al.[54] studied distributed monitoring for slope engineering, explaining Brillouin spectroscopy as the main point technique for developing the Brillouin optical time-domain reflectometer (BOTDR). It is enabled to measure strain generated in optical fibers as distributed in the longitudinal direction by optical time-domain reflectometry (ODTR).[55] Indeed, when the optical fiber is strained in the longitudinal direction, the backscattered light of Brillouin is subjected to a frequency shift proportional to the strain. Equation (3) expresses the Brillouin frequency shift as a function of the strain ε

$$v_B(\varepsilon) = v_B(0) + \frac{\delta v_B(\varepsilon)}{\delta \varepsilon} \cdot \varepsilon \tag{3}$$

where $v_B(\varepsilon)$ is the current Brillouin frequency; $v_B(0)$ is the reference Brillouin frequency; and $\delta v_B(\varepsilon)/\delta\varepsilon$ is the proportional coefficient of strain. One of the main advantages of BOTDR systems, compared with others, consists in the pulse light launched into one end of an optical fiber and the Brillouin backscattered light that can be detected at the same end. The BOTDR detection principle can be summarized in the following way: the laser light source emits a continuous light that can be separated into the probe light to the optical fiber output and the reference light for heterodyne detection. Then, an intensity modulator adapts the probe light into the pulse light, so the Brillouin backscattered light takes place as the pulse light launched into the optical fiber interacts with the acoustic phonons, and the frequency shift of Brillouin backscattered light occurs compared with the frequency of the launched pulse light. The frequency shift amount is proportional to the longitudinal strain of the optical fiber. Figure 3 summarizes the functioning and the measurement diagrams of the BOTDR system. A frequency shift is detected between positions z_1 and z_2 where the strain is located.

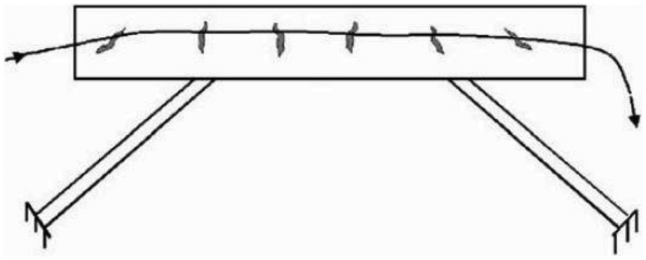

Fig. 2—Idealized rendering of fiber-optic sensors in civil infrastructures.[43]

Although sensitive along the entire length, the FOSs measure at discrete points that are spaced by a constant value called the sampling interval (SI), and the measured parameter (for example, strain) is averaged over a selected averaging length, spatial resolution (SR), which is dependent on the capabilities of the specific BOTDR system employed (Fig. 4). The averaged strain over the SR of the Brillouin-based systems is described as[56]

$$\bar{\varepsilon}_i = \frac{1}{d} \sum_{-d/2}^{d/2} \varepsilon_i(s) \cdot \delta_s \tag{4}$$

where $\bar{\varepsilon}_i$ is the weighted average strain at sampling point i; d is the SR or the length over which the BOTDR system averages the strain; s is the spatial distance along the fiber; δ_s is the increment between measured strain locations; and $\varepsilon_i(s)$ is the actual strain at a distance, s, from the section under consideration. Therefore, distributed FOSs provide the same information as discrete sensors in an equally spaced layout.[57] The wider the spatial resolution, the more the measurement of imperfections and inhomogeneities is attenuated, and therefore it is more difficult to identify them. This can be advantageous for inhomogeneous materials. However, if the goal of the SHM system is to detect local defects such as small cracks, then a small spatial resolution would be useful. Obviously, the size of the monitored structure also

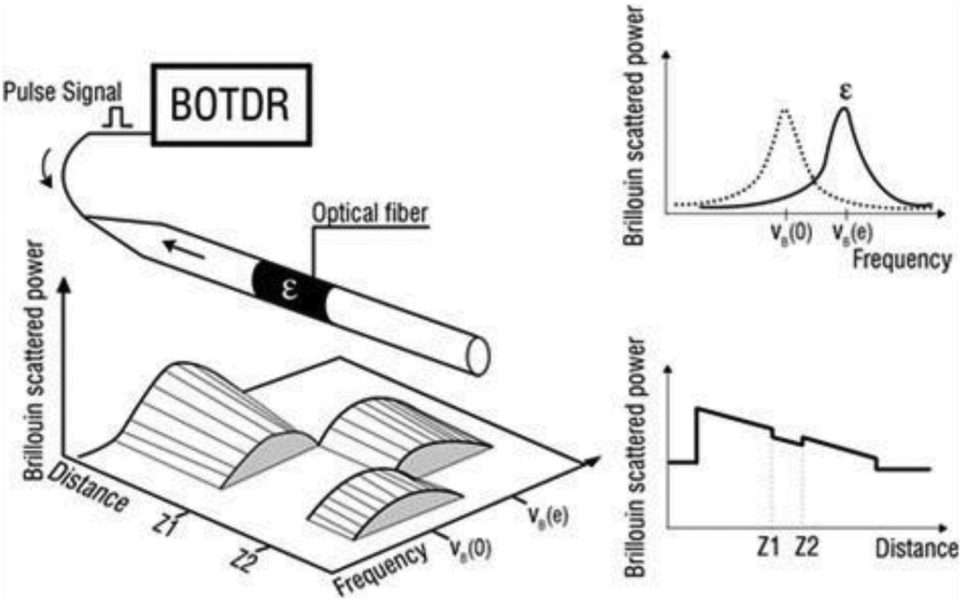

Fig. 3—Functioning and measurement diagrams of BOTDR system.

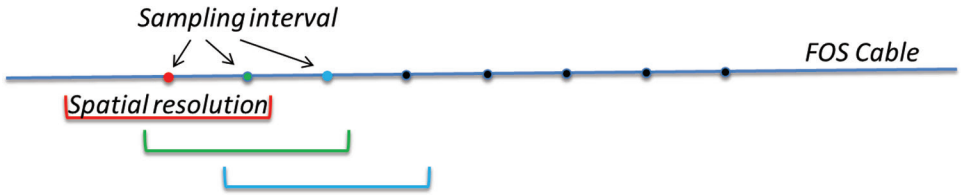

Fig. 4—Spatial resolution and sampling interval of BOTDR.

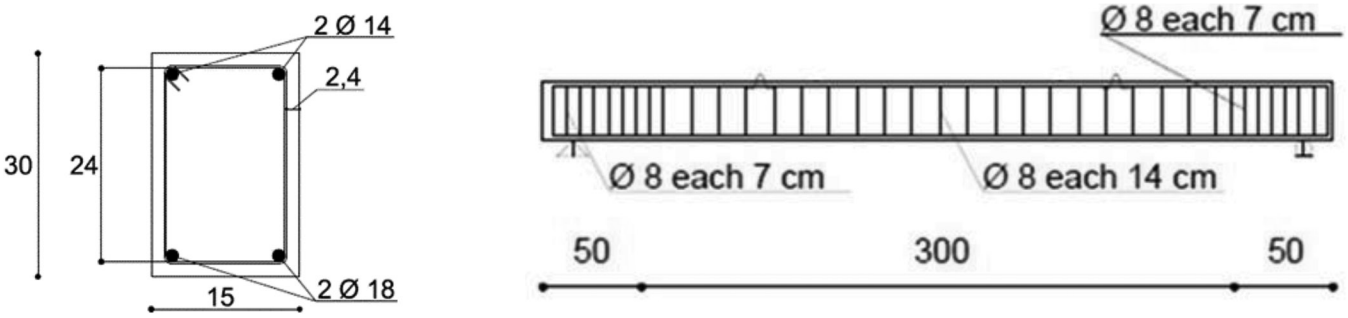

Fig. 5—Steel reinforcements: (a) cross section; and (b) longitudinal profile of beams.

affects the choice of SI and SR parameters, and a reasonable balance between monitoring system efficiency (for example, processing time and output size) and accuracy is a relevant issue for field applications. BOTDR measurements are also sensitive to temperature variations, so if the structure is subjected to both strain and temperature variations a temperature correction is applied. In the case of laboratory tests at constant temperature, this is not necessary.

Design of beam

Two RC beam specimens were designed to show ductile behavior with a progressive and gradual propagation of cracks under four-point monotonic loading conditions. The cross section was 150 mm wide and 300 mm high. The longitudinal steel reinforcements consisted of two bars of 14 mm diameter in the compressive region and two bars of 18 mm diameter in the tensile one. Stirrups of 8 mm diameter as shear reinforcements were installed with 70 mm spacing from the bearings to 500 mm. In the central portion of the beam, the shear reinforcements were installed with 140 mm spacing (Fig. 5). Concrete and steel materials have been selected adopting C20/25 and B450C types, respectively.[58]

Both Beams 1 and 2 have the same design. However, in Beam 1, two notches in the concrete cover were positioned at 1530 mm from the bearings to facilitate cracks at that positions, while, for Beam 2, a section at 20 cm from the midspan was weakened by halving the cross section of the longitudinal reinforcements to initiate the main crack in that position. The schematic plan of the notches with the general scheme of the four-point bending tests is shown in Fig. 6.

Random speckle pattern

The random speckle pattern was imposed on the lateral surface of the beam specimens within the midspan region of the beams (750 mm on each side) using different techniques of black and white paint. On Beam 1, the pattern was prepared manually, varnishing the lateral face with white color and then punctuating with a felt-tip pen. On the contrary, on Beam 2, a random-based algorithm was used to generate an automatic pattern. Then a solid template (a stencil) was made by a 3-D printing procedure to apply the numerically processed pattern, spraying with black varnish (Fig. 7). Both patterns provided equivalent displacement and deformation fields using the same software package (NCORR[35,36]). The automatically generated pattern, however, had the advantage of being faster to apply after creating the reference solid template.

FOS installation and four-point bending test

Different types of FOSs were embedded in the specimens before concrete placing and afterwards glued onto the external surface of the beams once the beams completed the curing period. The first type (Sensor 1) is a unique FOS used for the evaluation of distributed strain and temperature over several kilometers, using different scattering technologies (Brillouin and Raman). It contains four single-mode and two multi-mode optical fibers embedded in plastic material. Sensor 2 is composed of two bonded and two free single-mode optical fibers protected by a polyethylene thermoplastic profile. Temperature measurements were made by free fibers (not physically attached to concrete), and strains by bonded fibers. Sensor 3 is a single-mode optical fiber embedded in a glass fiber-reinforced polymer/epoxy tape, typically used for surface installation or embedding directly into composites. Sensor 4 is an optical fiber in a plastic matrix with a high Young's modulus. The fifth and last sensor (Sensor 5) was exclusively employed for temperature measurement. Figure 8 depicts the configuration of sensors within the specimens, and Fig. 9 pertains to the test setup.

The embedded optical-fiber sensors within the concrete beam had a pretension to keep them in a straight line configuration along the beam axis. The cable sensors embedded near the top and bottom surfaces of the beam were held in place by connections to stirrups. The compressive strength of the concrete was determined by testing four cubic specimens per beam. The cubic specimens were 150 mm on each

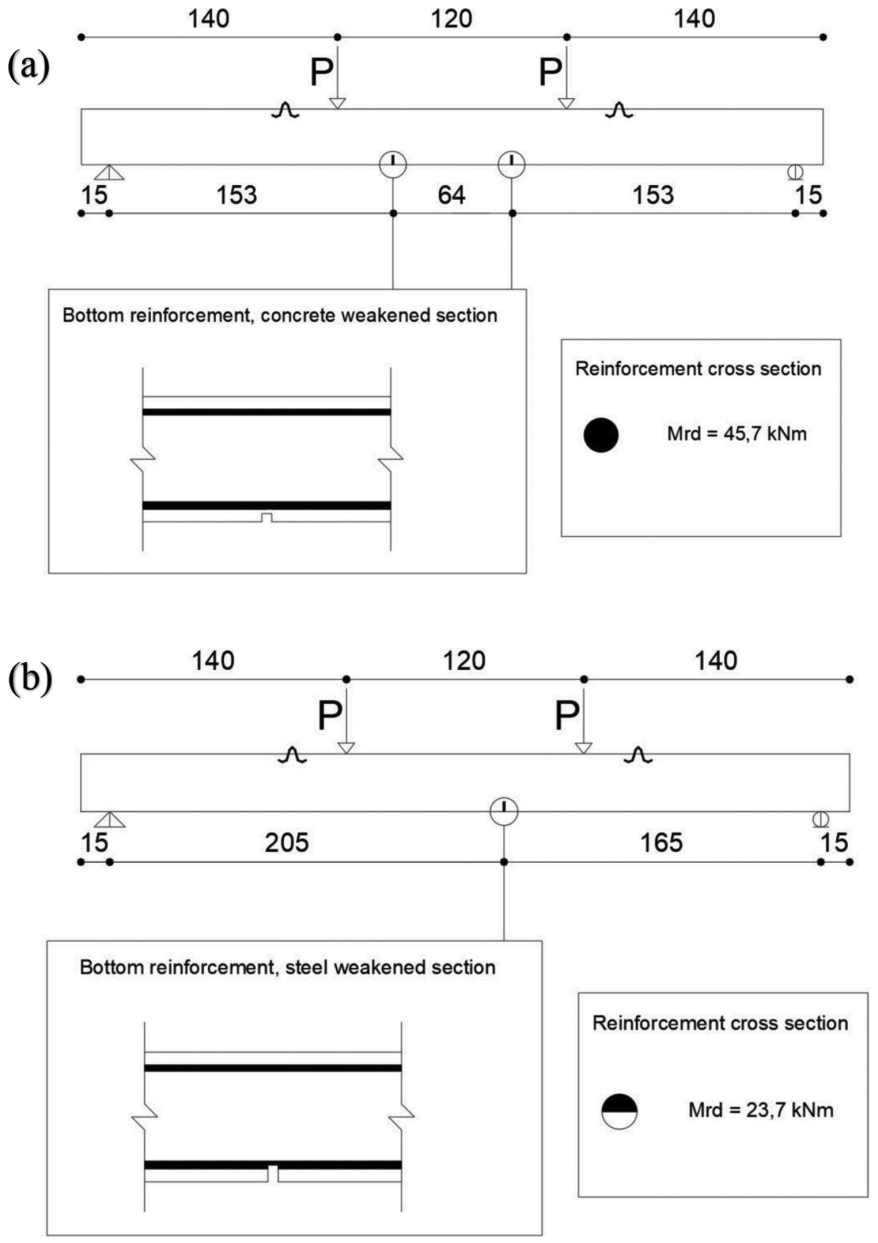

Fig. 6—(a) General scheme for four-point bending tests with positioning of notches for Beam 1; and (b) location of steel weakened section for Beam 2. (Note: Mrd is design bending moment.)

side and reached their ultimate compressive strength within the 500 to 600 kN range (Beam 1: Cube 1 was 550 kN, Cube 2 was 600 kN, Cube 3 was 500 kN, and Cube 4 was 550 kN; Beam 2: Cube 1 was 500 kN, Cube 2 was 600 kN, Cube 3 was 550 kN, and Cube 4 was 600 kN). It means a stress limit in the range of 22 to 26 MPa that is compatible with the concrete quality was selected during the design of the beams (C20/25). Figure 10 corresponds to a typical cube test for Beam 1.

After the preliminary materials characterization, the four-point bending tests were performed. The cracking and yielding loads were measured at 10 and 85 kN in comparison to the design estimates of 7 and 80 kN, respectively, for Beam 1. Beam 2 showed a lower strength and also a brittle behavior (Fig. 10), whereas Beam 1 showed a ductile response that allowed for capturing the progression and growth of the cracks. The crack paths at the completion of the Beam 1 test are shown in Fig. 11(a). Vertical cracks between the loading positions characterized the constant bending moment region, while 45-degree inclined cracks due to shear developed between the supports and loading points. Figure 11(c) depicts the global behavior of Beam 1: the horizontal plateau characterizing ductile behavior can be observed. The test was interrupted before the collapse. Figures 11(b) and (d) depict the main cracks of the weakened section for Beam 2 at failure and its brittle response in terms of the force-displacement curve, respectively.

RESULTS

Four-point bending tests in quasi-static conditions were performed on Beam 1 and 2, for which data was acquired by the proposed two-stage methodology. SR and SI were selected as those usually employed for field applications on real long-span structures (SR = 50 cm and SI = 20 cm)

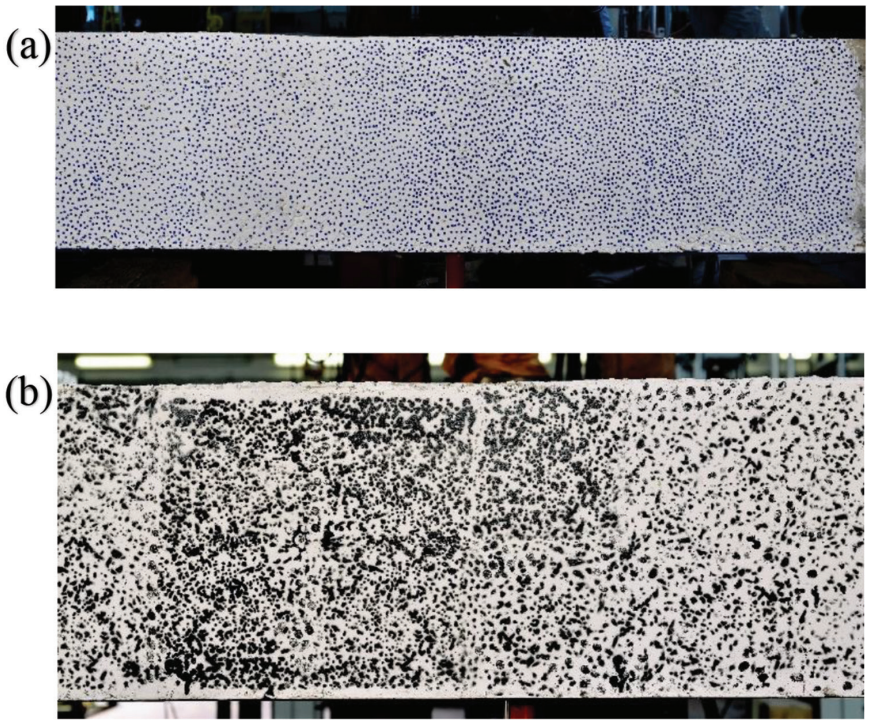

Fig. 7—Speckle patterns on: (a) Beam 1; and (b) Beam 2 lateral surface.

to detect and locate the unusual behavior due to cracking phenomena in the beam samples.

Figures 12(a) and (b) correspond to the increase in strain as a function of the increased load for Beams 1 and 2, respectively. The strain data shown in Fig. 12(a) and (b) were acquired by the distributed FOSs connected to the tension longitudinal steel reinforcements (refer also to the beams' global response in Fig. 11(c) and 11(d)). In Beam 1, which was designed to perform within the ductile domain, strains developed within the elastic range in the second load steps, with increased cracking in Load Steps 4 through 8, all the way to the yielding of reinforcements (Steps 10 to 12). However, the cracking propagation is mainly highlighted at the highest loading values (Steps 10 to 12), while at lower values incipient concentration of strain is evident in Step 8.

Crack quantification was performed by analyzing the region within the central span of Beam 1 by the DIC technique. Figure 12(c) corresponds to Load Step 12, where several cracks developed with a strain intensity of the same order of magnitude as those in Fig. 12(a). DIC results allow for accurate quantification of the cracks—that is, for the same load step, two cracks are evident in Fig. 12(c), at 30 and 45 cm, respectively, from the midspan at strain levels of 7000 με.

Figure 12(b) pertains to the distributed strains for Beam 2, which are characterized by the weakened section. FOS results allowed detection and location of the concentrated crack from Steps 6 to 8. During the same steps, measurements by DIC enable quantification of the main crack at the weakened section at a strain value of 12,000 με.

For both tested beams, FOSs installed on the reinforcements were able to locate damages exclusively at the highest loading values. This peculiar behavior can be related to their installation. Indeed, they were placed loose—that is, the optical fiber sensors were not pretensioned along their lengths. On the contrary, FOS cables positioned in the concrete bulk that have been installed with pretension detected the cracks even at lower loading levels. This is demonstrated in Fig. 13(a) for Beam 2, where the clear peak at Step 4 identifies the concentrated crack opening at the weakened section. At higher loading steps (6 to 8), this effect was still present but averaged by the development of additional cracks within the measurement SR that made it less evident.

Strains within the compression section of Beam 1 are shown in Fig. 13(b). The measured distributed strains correspond to the FOSs attached to the compression reinforcing bars. The development of higher compressive strains is evidenced at sections along the reinforcing bar, where tensile cracks had progressed further up towards the compression zone (Fig. 12(a) and (b)).

External FOS cables glued on the bottom side of beams allowed an accurate crack detection and location as well. Figure 14 reports the results for Beam 2, as measured by three different sensors (Sensors 1, 2, and 3). All three sensor types were able to detect and locate the crack openings, as shown in Fig. 14(a) to (c). Damage locations were verified by the concentrated strain regions by DIC. The first crack in Fig. 14(d), at approximately 2000 με, propagated, and then it was complemented by other cracks of lower intensity (Fig. 14(e) and (f)). From Step 3 to 4, cracks at the midspan region of Beam 2 doubled their intensity.

CONCLUSIONS

The development of a two-stage structural health monitoring (SHM) method for damage detection, location, and quantification in concrete structural elements was presented. It integrates the use of distributed fiber-optic sensors (FOSs)

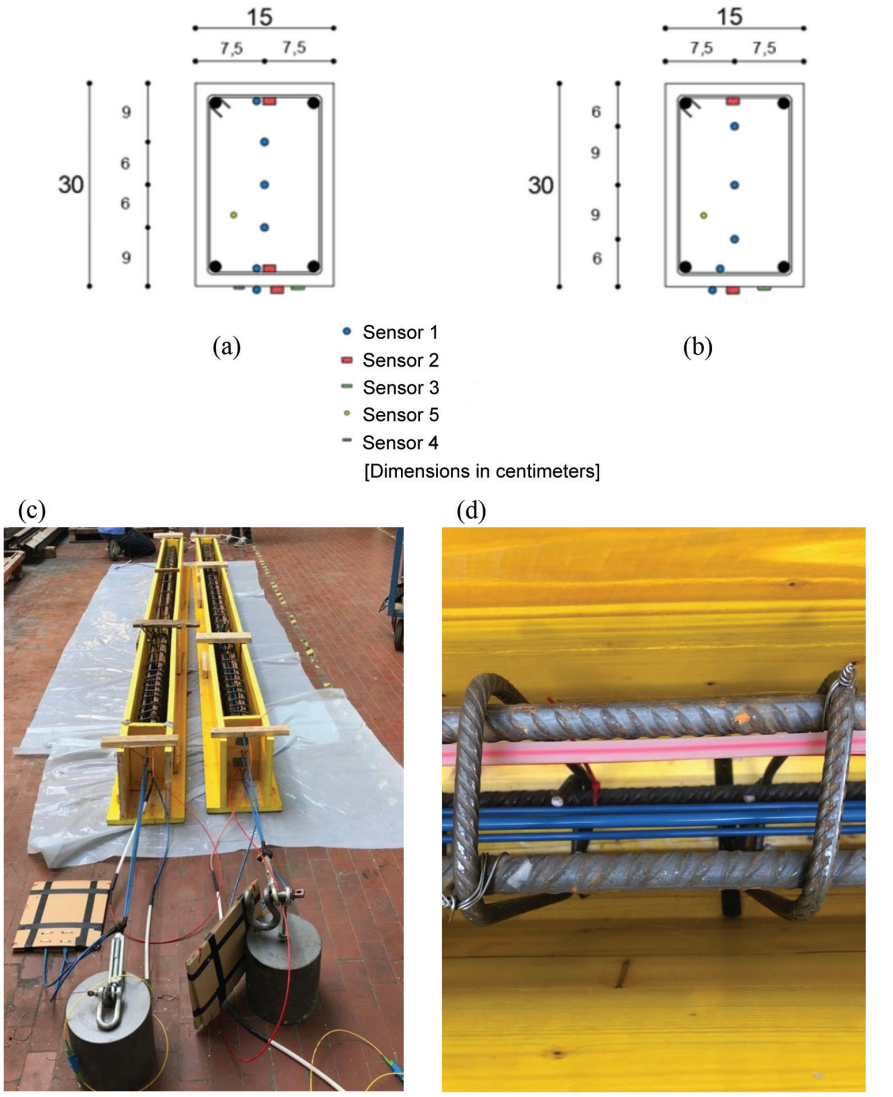

Fig. 8—FOS arrangement in cross sections: (a) Beam 1; and (b) Beam 2; (c) beam preparation with formwork; and (d) top view detail of longitudinal and transversal reinforcements with embedded FOSs.

Fig. 9—Test setup.

over an entire structure with local digital image correlation (DIC) measures. To evaluate the proposed method, two reinforced concrete (RC) beams were tested in the laboratory, installing FOSs in different positions to collect longitudinal strain measures. The sensors were: 1) embedded within the concrete; 2) connected to the longitudinal steel reinforcements; and 3) glued onto the external surfaces of the reinforced concrete beams. The fiber-optic interrogator had the characteristics of those employed for field applications, with spatial resolution (SR) and sampling interval (SI) that cannot

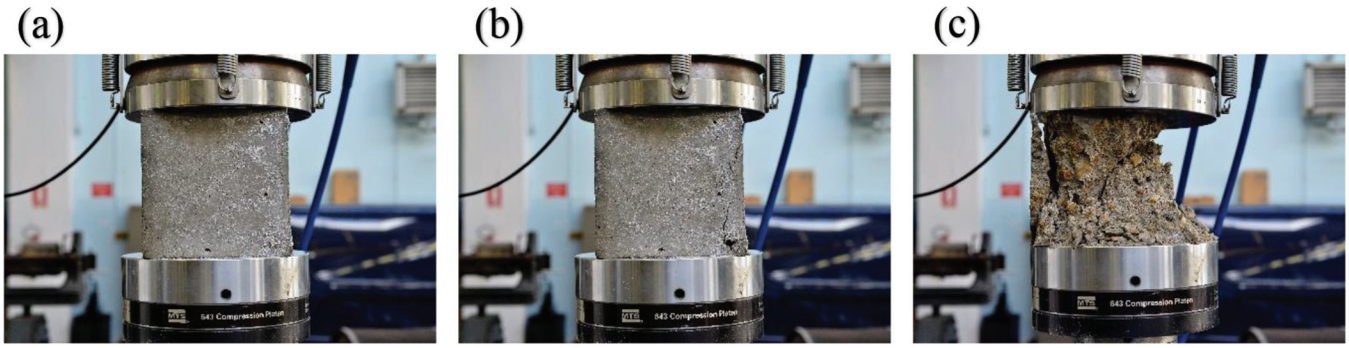

Fig. 10—Cube 3 beam compression test: (a) Step 1; (b) Step 4; and (c) Step 6.

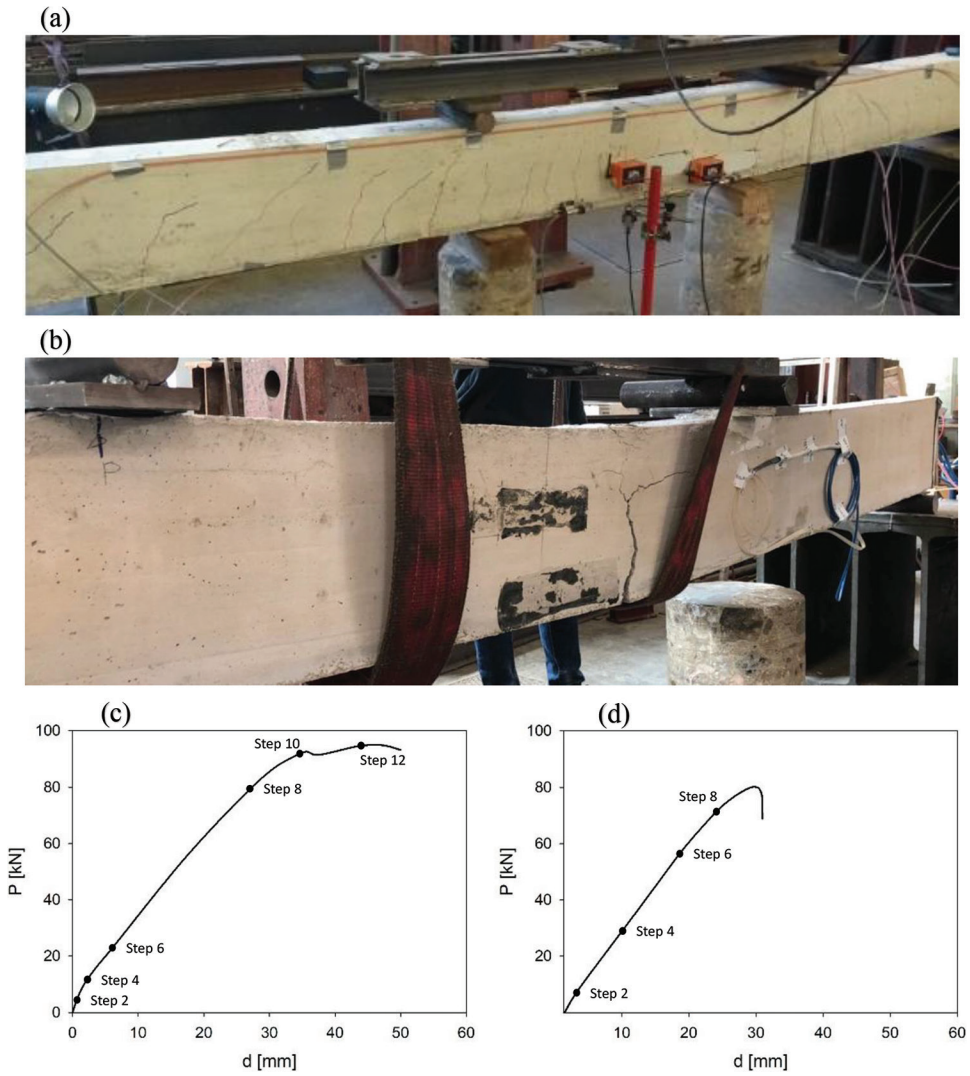

Fig. 11—(a) Crack path of Beam 1 at end of test, before collapse; (b) crack path of Beam 2 at collapse; force-displacement diagrams for (c) Beam 1; and (d) Beam 2.

directly give accurate information about damage quantification. To improve the SHM process, the DIC technique was adopted in a second stage in the area where the FOS system located the unusual behavior that could be related to cracking phenomena.

The beam samples were tested through four-point bending experiments. Beam 1 was designed to show a ductile response, and Beam 2 was characterized by a weakened section at 20 cm from the midspan. The FOS cables on the tension steel reinforcements were installed without any pretensioning. For both Beams 1 and 2, they were able to identify the crack openings at the highest loading conditions, beyond the yield strength limit of the steel reinforcing bars. On the other hand, the pretensioned FOS cables embedded within the concrete core in the tension zone were able to identify the crack openings, even at lower load values.

Three different surface-mounted FOSs were also employed to identify unusual behaviors in the concrete beams, and

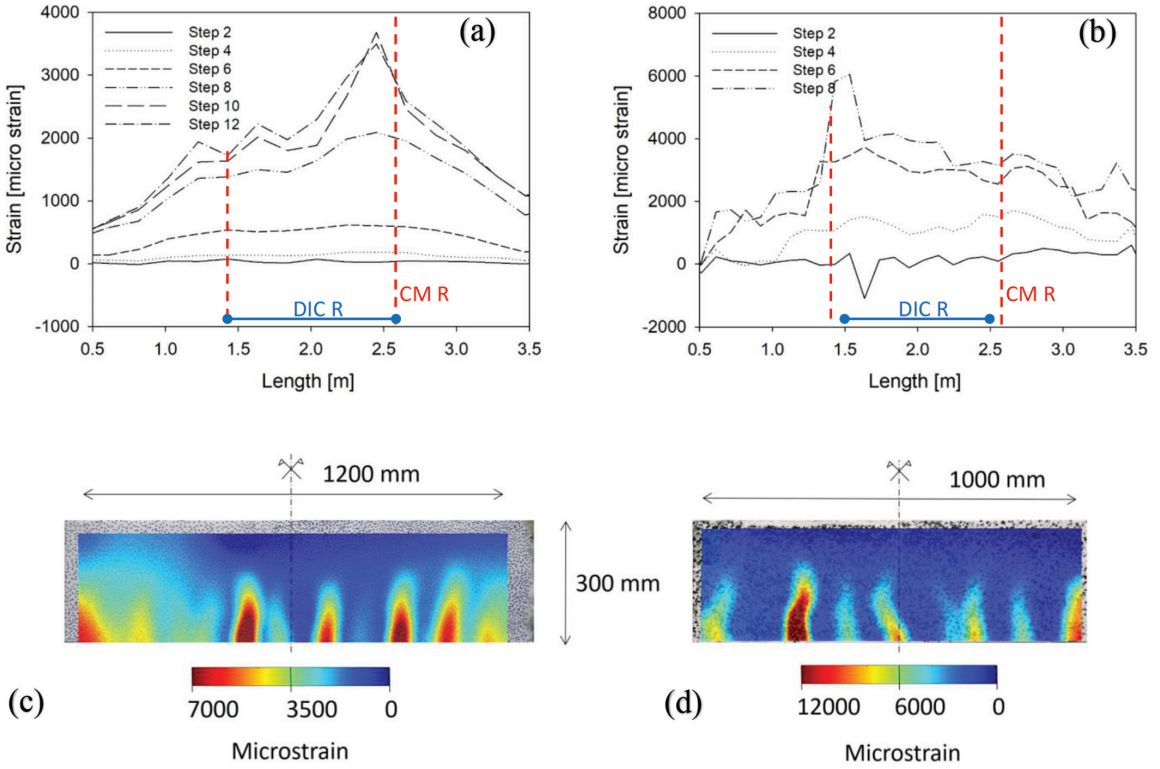

Fig. 12—Strain measures: FOSs at bottom longitudinal bars for (a) Beam 1; and (b) Beam 2; (c) DIC Step 12, Beam 1; and (d) DIC Step 8, Beam 2. (Note: CM R is constant moment region; DIC R is DIC region.)

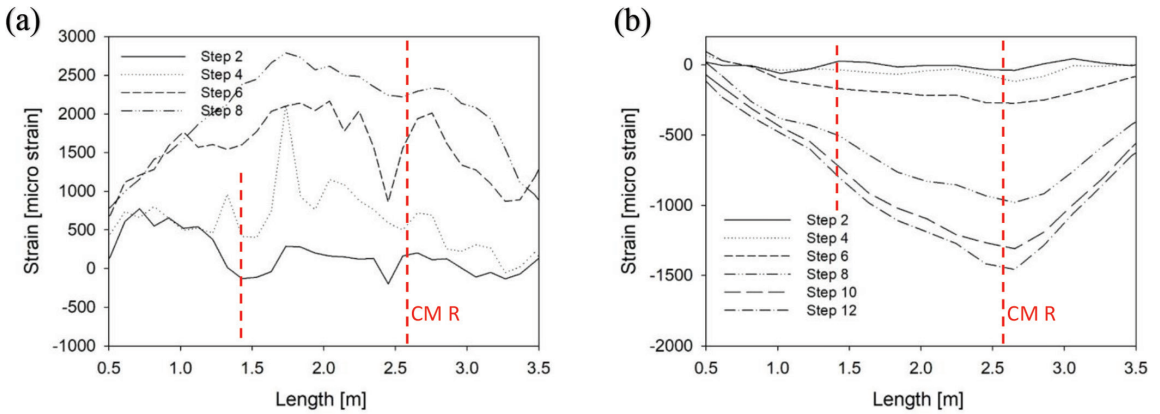

Fig. 13—Strain measures: (a) FOS at bottom concrete bulk of Beam 2; and (b) steel reinforcements at top of Beam 1. (Note: CM R is constant moment region.)

they were able to detect and locate the opening of the cracks from their early stages of development.

The DIC technique was then applied to the area where the FOSs identified the unusual behavior. The results confirmed the presence of cracks with satisfactory accuracy in terms of detection and quantification of cracks from their earlier development when they were undetectable to a visual inspection.

The proposed two-stage SHM method for damage identification proved effective in laboratory RC specimens for detecting, locating, and quantifying the presence of cracks of the same size as those that can be measured in real conditions on concrete structures of large dimensions. Furthermore, monitoring systems of the same class used for real structures were employed in the laboratory study. However, DIC, as presented and employed in the current application, is not practical for field applications in civil structures. Its use in the current application is limited to laboratory-controlled experiments for verification of the integrated use with distributed FOSs. Therefore, further developments on full-scale structures such as tunnel linings or long-span bridges will be needed.

AUTHOR BIOS

Maurizio Morgese *is a PhD Student at the University of Illinois Chicago, Chicago, IL. He received his BS and MS in civil engineering from the Politecnico di Torino, Turin, Piedmont, Italy, in 2016 and 2019, respectively. His research interests include structural engineering, structural health monitoring, and estimation of the remaining service life of concrete bridges.*

Marco Domaneschi *is an Assistant Professor at the Politecnico di Torino. He received his MS and PhD in civil structural engineering from the*

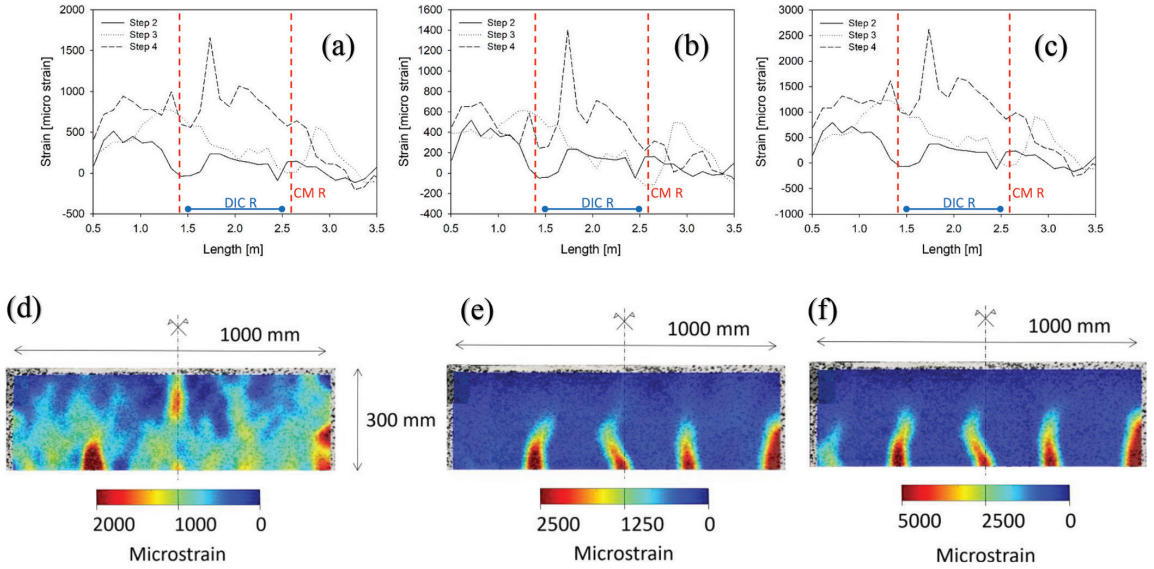

Fig. 14—Strain measures for Beam 2. FOSs at bottom external surface: (a) Sensor 3; (b) Sensor 2; and (c) Sensor 1; DIC output at (d) Step 2; (e) Step 3; and (f) Step 4. (Note: CM R is constant moment region; DIC R is DIC region.)

University of Pavia, Pavia, Lombardy, Italy, in 1998 and 2006, respectively. His research interests include structural engineering, finite element analysis of structures, and structural health monitoring.

Farhad Ansari *is a Distinguished Professor of civil engineering at the University of Illinois Chicago. He received his BS in civil engineering from the University of Illinois at Urbana-Champaign, Urbana, IL, in 1976; his MS in civil engineering from the University of Colorado, Denver, CO, in 1978; and his PhD from the University of Illinois Chicago in 1983. His research interests include structural engineering, structural health monitoring, and fiber-optic sensors.*

Gian Paolo Cimellaro *is a Full Professor at the Politecnico di Torino. He received his BS in civil engineering from the University of Rome "La Sapienza," Rome, Italy, in 2001, and his MS and PhD from the University at Buffalo, Buffalo, NY, in 2005 and 2008, respectively. His research interests include structural dynamics and earthquake engineering, disaster resilience, and structural health monitoring.*

Daniele Inaudi *is Co-Founder and CTO of SMARTEC SA and CTO of Roctest. He received a degree in physics from the Swiss Federal Institute of Technology, Zürich, Switzerland; his PhD in civil engineering from the IMAC Laboratory of Stress Analysis of the Swiss Federal Institute of Technology, Lausanne, Switzerland, in 1997; and his master's in business administration from the University of Applied Sciences and Arts of Southern Switzerland, Manno, Switzerland, in 2005.*

ACKNOWLEDGMENTS

This research has received funding from the European Research Council under the Grant Agreement No. ERC_IDEAL RESCUE_637842 of the project IDEal reSCUE—Integrated Design and Control of Sustainable Communities during Emergencies. The technical support of SMARTEC (Switzerland) and MastrLab at Politecnico di Torino – DISEG is gratefully acknowledged. R. Belli (SMARTEC) installed the distributed fiber-optic sensors and supported the system setup; his contribution is also gratefully acknowledged.

REFERENCES

1. Gkoumas, K.; Marques Dos Santos, F. L.; Van Balen, M.; Tsakalidis, A.; Ortega Hortelano, A.; Grosso, M.; Haq, A.; and Pekar, F., "Research and Innovation in Bridge Maintenance, Inspection and Monitoring," EUR 29650 EN, Publications Office of the European Union, Luxembourg, 2019. doi: 10.2760/06996710.2760/069967

2. Richard Pérez-Peña, "After Italy Collapse, Europe Asks: How Safe Are Our Bridge?" *The New York Times*, https://www.nytimes.com/2018/08/21/world/europe/genoa-bridge-collapse.html. (last accessed Sept. 1, 2021)

3. Nagarajaiah, S., and Erazo, K., "Structural Monitoring and Identification of Civil Infrastructure in the United States," *Structural Monitoring and Maintenance*, V. 3, No. 1, 2016, pp. 51-69. doi: 10.12989/smm.2016.3.1.051

4. Valigura, J.; Liel, A. B.; and Sideris, P., "Risk-Based Assessment of Seismic Repair Costs for Reinforced Concrete Bridges Considering Competing Repair Strategies," *Journal of Bridge Engineering*, ASCE, V. 24, No. 11, 2019, p. 04019108. doi: 10.1061/(ASCE)BE.1943-5592.0001466

5. Cimellaro, G. P.; Scura, G.; Renschler, C. S.; Reinhorn, A. M.; and Kim, H. U., "Rapid Building Damage Assessment System Using Mobile Phone Technology," *Earthquake Engineering and Engineering Vibration*, V. 13, No. 3, 2014, pp. 519-533. doi: 10.1007/s11803-014-0259-4

6. Morgese, M.; Ansari, F.; Domaneschi, M.; and Cimellaro, G. P., "Post-Collapse Analysis of Morandi's Polcevera Viaduct in Genova Italy," *Journal of Civil Structural Health Monitoring*, V. 10, No. 1, 2020, pp. 69-85. doi: 10.1007/s13349-019-00370-7

7. Glisic, B., "Long-Term Monitoring of Civil Structures and Infrastructure Using Long-Gauge Fiber Optic Sensors," *18th IEEE Sensors*, SENSORS 2019, Montreal, QC, Canada, 2019

8. Unger, J. F.; Teughels, A.; and De Roeck, G., "System Identification and Damage Detection of a Prestressed Concrete Beam," *Journal of Structural Engineering*, ASCE, V. 132, No. 11, 2006, pp. 1691-1698. doi: 10.1061/(ASCE)0733-9445(2006)132:11(1691)

9. Oskoui, E. A.; Taylor, T.; and Ansari, F., "Method and Monitoring Approach for Distributed Detection of Damage in Multi-Span Continuous Bridges," *Engineering Structures*, V. 189, June 2019, pp. 385-395. doi: 10.1016/j.engstruct.2019.02.037

10. Casas, J. R., and Cruz, P. J. S., "Fiber Optic Sensors for Bridge Monitoring," *Journal of Bridge Engineering*, ASCE, V. 8, No. 6, 2003, pp. 362-373. doi: 10.1061/(ASCE)1084-0702(2003)8:6(362)

11. Barrias, A.; Rodriguez, G.; Casas, J. R.; and Villalba, S., "Application of Distributed Optical Fiber Sensors for the Health Monitoring of Two Real Structures in Barcelona," *Structure and Infrastructure Engineering*, V. 14, No. 7, 2018, pp. 967-985. doi: 10.1080/15732479.2018.1438479

12. Güemes, A.; Fernández-López, A.; and Soller, B., "Optical Fiber Distributed Sensing – Physical Principles and Applications," *Structural Health Monitoring*, V. 9, No. 3, 2010, pp. 233-245. doi: 10.1177/1475921710365263

13. Talebinejad, I.; Fischer, C.; and Ansari, F., "A Hybrid Approach for Safety Assessment of Double Span Masonry Vaults of the Brooklyn Bridge," *Journal of Civil Structural Health Monitoring*, V. 1, No. 1-2, 2011, pp. 3-15. doi: 10.1007/s13349-011-0003-y

14. Li, H.-N.; Li, D.-S.; and Song, G.-B., "Recent Applications of Fiber Optic Sensors to Health Monitoring in Civil Engineering," *Engineering Structures*, V. 26, No. 11, 2004, pp. 1647-1657. doi: 10.1016/j.engstruct.2004.05.018

15. Oskoui, E. A.; Taylor, T.; and Ansari, F., "Reference-Free Dynamic Distributed Monitoring of Damage in Multispan Bridges," *Journal of Structural Engineering*, ASCE, V. 147, No. 1, 2021, p. 04020292. doi: 10.1061/(ASCE)ST.1943-541X.0002858

16. Bien, J.; Elfgren, L.; and Olofsson, J., eds., *Sustainable Bridges. Assessment for Future Traffic Demands and Longer Lives*, Dolnoslaskie Wydawnictwo Edukacyjne, Wrocław, Poland, 2007, 490 pp.

17. Limongelli, M. P., and Orcesi, A., "Report of the Innovation Task Group: COST TU 1406, Quality Specifications for Roadway Bridges,"

Eurostruct, Guimarães, Portugal, 2019, 94 pp., https://eurostruct.org/repository/tu1406-report-innovation-subgroup-v2.pdf.

18. Ramos, T.; Furtado, A.; Eslami, S.; Alves, S.; Rodrigues, H.; Arêde, A.; Tavares, P. J.; and Moreira, P. M. G. P., "2D and 3D Digital Image Correlation in Civil Engineering – Measurements in a Masonry Wall," *Procedia Engineering*, V. 114, 2015, pp. 215-222. doi: 10.1016/j.proeng.2015.08.061

19. Yue, J. G.; Kunnath, S. K.; and Xiao, Y., "Uniaxial Concrete Tension Damage Evolution Using Acoustic Emission Monitoring," *Construction and Building Materials*, V. 232, Jan. 2020, p. 117281. doi: 10.1016/j.conbuildmat.2019.117281

20. Nonis, C.; Niezrecki, C.; Yu, T.-Y.; Ahmed, S.; Su, C.-F.; and Schmidt, T., "Structural Health Monitoring of Bridges using Digital Image Correlation," *Health Monitoring of Structural and Biological Systems 2013*, *Proceedings*, V. 8695, Apr. 2013, 13 pp. doi: 10.1117/12.2009647

21. Mahal, M.; Blanksvärd, T.; Täljsten, B.; and Sas, G., "Using Digital Image Correlation to Evaluate Fatigue Behavior of Strengthened Reinforced Concrete Beams," *Engineering Structures*, V. 105, 2015, pp. 277-288. doi: 10.1016/j.engstruct.2015.10.017

22. Sas, G.; Blanksvärd, T.; Enochsson, O.; Täljsten, B.; and Elfgren, L., "Photographic Strain Monitoring During Full-Scale Failure Testing of Örnsköldsvik Bridge," *Journal of Structural Health Monitoring*, V. 11, No. 4, 2012, pp. 489-498. doi: 10.1177/1475921712438568

23. Scarella, A.; Salamone, G.; Babanajad, S. K.; De Stefano, A.; and Ansari, F., "Dynamic Brillouin Scattering-Based Condition Assessment of Cables in Cable-Stayed Bridges," *Journal of Bridge Engineering*, ASCE, V. 22, No. 3, 2017, p. 04016130. doi: 10.1061/(ASCE)BE.1943-5592.0001010

24. Domaneschi, M.; Pellecchia, C.; De Iuliis, E.; Cimellaro, G. P.; Morgese, M.; Khalil, A. A.; and Ansari, F., "Collapse Analysis of the Polcevera Viaduct by the Applied Element Method," *Engineering Structures*, V. 214, 2020, p. 110659. doi: 10.1016/j.engstruct.2020.110659

25. Peters, W. H., and Ranson, W. F., "Digital Imaging Techniques in Experimental Stress Analysis," *Optical Engineering*, V. 21, No. 3, 1982, p. 213427. doi: 10.1117/12.7972925

26. Sutton, M. A.; Mingqi, C.; Peters, W. H.; Chao, Y. J.; and McNeill, S. R., "Application of an Optimized Digital Correlation Method to Planar Deformation Analysis," *Image and Vision Computing*, V. 4, No. 3, 1986, pp. 143-150. doi: 10.1016/0262-8856(86)90057-0

27. Hild, F., and Roux, S., "Digital Image Correlation: from Displacement Measurement to Identification of Elastic Properties—a Review," *Strain*, V. 42, No. 2, 2006, pp. 69-80. doi: 10.1111/j.1475-1305.2006.00258.x

28. Roux, S.; Réthoré, J.; and Hild, F., "Recent Progress in Digital Image Correlation: From Measurement to Mechanical Identification," *Journal of Physics: Conference Series 135*, 6th International Conference on Inverse Problems in Engineering: Theory and Practice, Dourdan, France, 2008, 9 pp.

29. Pan, B.; Qian, K.; Xie, H.; and Asundi, A., "Two-Dimensional Digital Image Correlation for In-Plane Displacement and Strain Measurement: A Review," *Measurement Science and Technology*, V. 20, No. 6, 2009, p. 062001. doi: 10.1088/0957-0233/20/6/062001

30. Wu, L.-J.; Casciati, F.; and Casciati, S., "Dynamic Testing of a Laboratory Model via Vision-Based Sensing," *Engineering Structures*, V. 60, Feb. 2014, pp. 113-125. doi: 10.1016/j.engstruct.2013.12.002

31. Dworakowski, Z.; Kohut, P.; Gallina, A.; Holak, K.; and Uhl, T., "Vision-Based Algorithms for Damage Detection and Localization in Structural Health Monitoring," *Structural Control and Health Monitoring*, V. 23, No. 1, May 2015, pp. 35-50.

32. Feng, D., and Feng, M. Q., "Computer Vision for SHM of Civil Infrastructure: From Dynamic Response Measurement to Damage Detection – A Review," *Engineering Structures*, V. 156, Feb. 2018, pp. 105-117. doi: 10.1016/j.engstruct.2017.11.018

33. Niezrecki, C.; Baqersad, J.; and Sabato, A., "Digital Image Correlation Techniques for NDE and SHM," *Handbook of Advanced Non-Destructive Evaluation*, Springer, 2018, pp. 1-46.

34. Pan, B., "Digital Image Correlation for Surface Deformation Measurement: Historical Developments, Recent Advances and Future Goals," *Measurement Science and Technology*, V. 29, No. 8, 2018, p. 082001. doi: 10.1088/1361-6501/aac55b

35. Tang, Z.-Z.; Liang, J.; Xiao, Z.-Z.; Guo, C.; and Hu, H., "Three-Dimensional Digital Image Correlation System for Deformation Measurement in Experimental Mechanics," *Optical Engineering*, V. 49, No. 10, 2010, p. 103601. doi: 10.1117/1.3491204

36. Blaber, J.; Adair, B.; and Antoniou, A., "Ncorr: Open-Source 2D Digital Image Correlation Matlab Software," *Experimental Mechanics*, V. 55, No. 6, July 2015, pp. 1105-1122.

37. Sutton, M. A.; McNeill, S. R.; Helm, J. D.; and Chao, Y. J., "Advances in Two-Dimensional and Three-Dimensional Computer Vision," *Photomechanics. Topics in Applied Physics*, V. 77, Springer, 2000, pp 323-372.

38. Luo, P. F.; Chao, Y. J.; Sutton, M. A.; and Peters, W. H., III, "Accurate Measurement of Three-Dimensional Deformations in Deformable and Rigid Bodies Using Computer Vision," *Experimental Mechanics*, V. 33, No. 2, 1993, pp. 123-132. doi: 10.1007/BF02322488

39. Helm, J. D.; McNeill, S. R.; and Sutton, M. A., "Improved Three-Dimensional Image Correlation for Surface Displacement Measurement," *Optical Engineering*, V. 35, No. 7, 1996, p. 1911. doi: 10.1117/1.600624

40. Garcia, D.; Orteu, J. J.; and Penazzi, L., "A Combined Temporal Tracking and Stereo-Correlation Technique for Accurate Measurement of 3D Displacement: Application to Sheet Metal Forming," *Journal of Materials Processing Technology*, V. 125-126, Sept. 2002, pp. 736-742. doi: 10.1016/S0924-0136(02)00380-1

41. Pan, B.; Xie, H. M.; Yang, L. H.; and Wang, Z. Y., "Accurate Measurement of Satellite Antenna Surface Using 3D Digital Image Correlation Technique," *Strain*, V. 45, No. 2, 2009, pp. 194-200. doi: 10.1111/j.1475-1305.2008.00450.x

42. Zhang, D. S.; Luo, M.; and Arola, D. D., "Displacement/Strain Measurements Using an Optical Microscope and Digital Image Correlation," *Optical Engineering*, V. 45, No. 3, Mar. 2006, p. 2613.

43. Sutton, M. A.; Li, N.; Garcia, D.; Cornille, N.; Orteu, J. J.; McNeill, S. R.; Schreier, H. W.; and Li, X., "Metrology in a Scanning Electron Microscope: Theoretical Developments and Experimental Validation," *Measurement Science and Technology*, V. 17, No. 10, 2006, p. 2613. doi: 10.1088/0957-0233/17/10/012

44. Sutton, M. A.; Li, N.; Joy, D. C.; Reynolds, A. P.; and Li, X., "Scanning Electron Microscopy for Quantitative Small and Large Deformation Measurements Part I: SEM Imaging at Magnifications from 200 to 10,000," *Experimental Mechanics*, V. 47, No. 6, 2007, pp. 775-787. doi: 10.1007/s11340-007-9042-z

45. Sutton, M. A.; Li, N.; Garcia, D.; Cornille, N.; Orteu, J. J.; McNeill, S. R.; Schreier, H. W.; Li, X.; and Reynolds, A. P., "Scanning Electron Microscopy for Quantitative Small and Large Deformation Measurements Part II: Experimental Validation for Magnifications from 200 to 10,000," *Experimental Mechanics*, V. 47, No. 6, 2007, pp. 789-804. doi: 10.1007/s11340-007-9041-0

46. Sun, Y., and Pang, J. H. L., "AFM Image Reconstruction for Deformation Measurements by Digital Image Correlation," *Nanotechnology*, V. 17, No. 4, 2006, pp. 933-939. doi: 10.1088/0957-4484/17/4/016

47. Yoneyama, S.; Kikuta, H.; Kitagawa, A.; and Kitamura, K., "Lens Distortion Correction for Digital Image Correlation by Measuring Rigid Body Displacement," *Optical Engineering*, V. 45, No. 2, 2006, p. 023602. doi: 10.1117/1.2168411

48. Yoneyama, S.; Kitagawa, A.; Kitamura, K.; and Kikuta, H., "In-Plane Displacement Measurement Using Digital Image Correlation with Lens Distortion Correction," *JSME International Journal. Series A, Solid Mechanics and Material Engineering*, V. 49, No. 3, 2006, pp. 458-467. doi: 10.1299/jsmea.49.458

49. Ansari, F., "Application of Laser Speckle Interferometry to Fracture of Concrete," *Proceedings of the Society of Photo-Optical Instrumentation Engineers*, Southwest Conference on Optics, Albuquerque, NM, V. 0540, 1985, pp. 492-499.

50. Ansari, F., "Stress-Strain Response of Microcracked Concrete in Direct Tension," *ACI Materials Journal*, V. 84, No. 6, Nov.-Dec. 1987, pp. 481-490.

51. Ansari, F., "Mechanism of Microcracked Formation in Concrete," *ACI Materials Journal*, V. 86, No. 5, Sept.-Oct. 1989, pp. 459-464.

52. Pan, B.; Asundi, A.; Xie, H.; and Gao, J., "Digital Image Correlation Using Iterative Least Squares and Pointwise Least Squares for Displacement Field and Strain Field Measurements," *Optics and Lasers in Engineering*, V. 47, No. 7-8, 2009, pp. 865-874. doi: 10.1016/j.optlaseng.2008.10.014

53. Ansari, F., "Practical Implementation of Optical Fiber Sensors in Civil Structural Health Monitoring," *Journal of Intelligent Material Systems and Structures*, V. 18, No. 8, 2007, pp. 879-889. doi: 10.1177/1045389X06075760

54. Shi, B.; Sui, H.; Liu, J.; and Zhang, D., "The BOTDR-Based Distributed Monitoring System for Slope Engineering," *The Geological Society of London 2006*, IAEG2006 Paper No. 683.

55. Bao, X., and Chen, L., "Recent Progress in Brillouin Scattering Based Fiber Sensors," *Sensors (Basel)*, V. 11, No. 4, 2011, pp. 4152-4187. doi: 10.3390/s110404152

56. Nazarian, E.; Ansari, F.; Zhang, X.; and Taylor, T., "Detection of Tension Loss in Cable-Stayed Bridges by Distributed Monitoring of Bridge Deck Strains," *Journal of Structural Engineering*, ASCE, V. 142, No. 6, 2016.

57. Glišić, B., and Inaudi, D., *Fibre Optic Methods for Structural Health Monitoring*, John Wiley & Sons, Inc., New York, 2007, 276 pp.

58. "D. M. Aggiornamento delle Norme Tecniche per le Costruzioni [Updating of the Technical Standards for Construction, Italy]," *Gazzetta Ufficiale*, Jan. 17, 2018, 372 pp. (in Italian)